Journal of Geophysics, 61, 97-109.

# Audiomagnetotelluric sounding using the Schumann resonances

**A. Tzanis* and D. Beamish**
British Geological Survey, Murchison House, West Mains Road, Edinburgh EH9 3LA, United Kingdom

**Abstract.** The Schumann resonance waveforms in the lower ELF band (5–100 Hz) are produced within the Earth-ionosphere cavity by distant lightning discharges; they provide a useful source field for shallow audiomagnetotelluric (AMT) crustal sounding. In this study we investigate their waveform characteristics that are important to the assumptions of AMT sounding. A time-domain polarization analysis technique is applied to a variety of examples of Schumann resonance waveforms. The multiplicity of worldwide thunderstorm centres provides a background activity which is generally incoherent and, accordingly, displays incoherent polarization characteristics. Superimposed on the background are larger-amplitude transient events (sferics) from individual thunderstorm centres; they represent the response of the Earth-ionosphere cavity to very large lightning discharges and are generally linearly polarized at a given azimuth. The analysis indicates that the Schuman resonance waveforms provide a plane-wave source field, as required for electromagnetic crustal sounding. The differences in the "received" characteristics between the two waveform types prompted an investigation of the extent to which the waveform type and its particular polarization characteristics influence the determination of a geoelectric sounding curve. A detailed study, carried out with a multivariate maximum entropy spectral analysis algorithm, indicates that the two types of Schumann resonance waveform provide repeatable and consistent results at the 95% confidence level and that the linear polarizations associated with the sferics do not influence the estimation of the Earth response.

**Key words:** Electromagnetic induction – Audiomagnetotelluric – Schumann resonances Polarization analysis – Autoregressive spectral estimation

## Introduction

Audiomagnetotelluric (AMT) crustal sounding is an extension of the lower frequency ($f<1$ Hz) magnetotelluric (MT) method to higher frequencies. The basic requirement for both methods of geoelectric sounding is a time-varying electromagnetic source field. Such an external field provides the energy source for electromagnetic induction in the conducting Earth. The time variations are recorded as two components of the induced electric field ($E_x$, $E_y$) and the combined inducing and induced magnetic field ($H_x$, $H_y$) at a particular location. Linear relationships between the field components, calculated as a function of frequency, enable a geoelectric sounding curve to be obtained and interpreted. High-frequency source fields enable relatively shallow crustal targets to be explored. If the instrumental bandwidth extends to 100 Hz, skin depths would range from 158 m to 16 km in uniform crustal rocks with resistivities from 10 to $10^5$ ohm·m, respectively.

The transition frequency from MT to AMT sounding is not arbitrary (Keller, 1971). A frequency of several hertz is associated with a distinct minimum in the Earth's natural electromagnetic source spectrum (Watt, 1967). At frequencies of $f<1$ Hz the source fields are primarily of magnetospheric and ionospheric origin, i.e. associated with perturbations of the main geomagnetic field. The geomagnetic energy spectrum for $f<1$ Hz, observed in active regions of the magnetosphere, displays an approximately $f^{-2}$ to $f^{-3}$ dependence (Russell et al., 1970). This spectral decay, combined with the low energy transmission coefficient of the ionosphere at such frequencies (Abbas, 1968), suggests that only a few rare magnetospheric disturbance fields will contribute significant amounts of energy at frequencies greater than a few hertz. The natural noise spectrum in the 5 Hz–25 kHz range is primarily due to electromagnetic perturbations generated by lightning discharges (ELF sferics). Such sources may contain a wide spectrum of frequencies. However, for distant (i.e. worldwide) sources, the energy undergoes multiple reflection in the Earth-ionosphere waveguide giving rise to frequency-dependent attenuation. In the lower audio band (i.e. $f<2$ kHz) the energy propagates as a transverse magnetic mode in which the electric field is largely radial. The largest energy components in this lower audio band are the Schumann resonance modes. The first five of these modes have typical frequencies of 7.8, 14.1, 20.3, 26.3 and 32.5 Hz (Madden and Thomson, 1965). The present study considers some aspects of sferic source fields, in particular the Schumann resonance modes, and their utilisation in AMT crustal sounding.

Although AMT instrumentation may use the natural spectrum up to 10 kHz (Strangway et al., 1973), we confine our attention to the low-order Schumann resonance modes ($f<100$ Hz). Telluric and magnetotelluric prospecting methods, using the fundamental mode ($f=7.8$ Hz), have been described by Slankis et al. (1972). The analysis of the characteristics of audio signals described by Telford (1977) was undertaken using time-averaged measurements of the

induced electric field. This would appear to be the least effective way to determine the source characteristics of signals propagating in a transverse magnetic mode. Although AMT tensor measurements are now increasingly common, descriptions of source (and noise) characteristics are usually restricted to the spectral content of the waveforms (Hoover et al., 1978; Labson et al., 1985). In order to provide a more detailed description of typical source characteristics, we investigate here a useful method for the polarization analysis of sferic waveforms.

Common assumptions in both the MT and AMT methods are that the source field approximates an incident plane wave and that no current sources exist within the region through which electromagnetic induction takes place. It is quite possible for both of these assumptions to break down when we attempt to use sferic sources in the lower audio band (5 Hz–2 kHz). The plane-wave assumption is not appropriate for energy sources which derive from local and regional thunderstorm activity (examples are provided in Keller and Frischknecht, 1966). The power distribution grid and its users are capable of providing both narrow-band and broad-band current sources which invalidate the second assumption. The present study avoids the second complication by using "clean" Schumann resonance waveforms (Beamish and Tzanis, 1986). The first assumption is examined by considering the general characteristics of sferic sources across the Schumann bandwidth. A polarization analysis of the magnetic field components of Schumann resonance waveforms is then described and their ability to provide repeatable geoelectric sounding curves is then investigated.

## General characteristics of sferic sources

In the ELF band, electromagnetic energy is largely produced by radiation from vertical lightning discharges. Descriptions of the processes involved can be found in Uman (1969). For a particular model of the discharge (e.g. single or return strokes), the discharge will be characterized by its current moment (time domain) or equivalently by its source spectrum (frequency domain). The electric field energy generated comprises electrostatic, inductive and radiation components which decay with distance ($D$) as $1/D^3$, $1/D^2$ and $1/D$, respectively. The electrostatic term represents the dominant component up to distances of about 20 km, while the radiation term predominates at distances in excess of 100 km (Bliokh et al., 1980). In order to observe the Schumann resonances, we require that the source-receiver separation be large (e.g. $>1000$ km) and that the source provides forced oscillations within the Earth-ionosphere cavity. Under these circumstances, the received spectrum will be the product of the source spectrum and the waveguide transmission function.

The three main equatorial thunderstorm centres in Central/South America, Central Africa and S.E. Asia (Keller and Frischknecht, 1966) provide a nearly uniform source of ELF noise in that there exists a high probability that a thunderstorm is in progress somewhere on the globe. The presence of such recurring centres of activity suggests that mid- and high-latitude locations maintain a high probability of being in the far-field ($D>10000$ km) region with respect to the main source locations. In addition to this spatial distribution, thunderstorm activity can also be characterized by a time dependence. The broad feature of late afternoon maximum (20:00 U.T.) and a night-time minimum (04:00 U.T.) in ELF noise may be further developed by including the time-dependent contributions from the three main thunderstorm centres. The activity of these centres, as a function of universal time, is reproduced from Bliokh et al. (1980) in Fig. 1. In this *statistical* model, ELF energy would be received from each of the three centres during the course of the day.

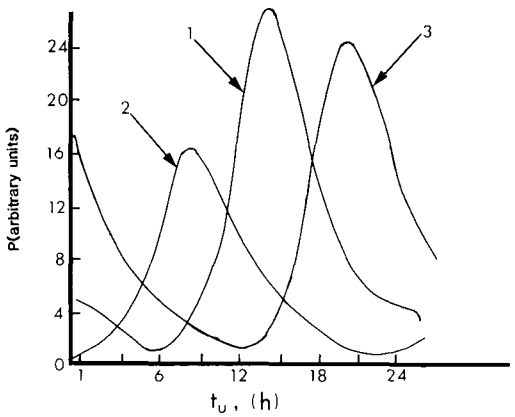


**Fig. 1.** Lightning activity of the global thunderstorm centres as a function of universal time. (1) African centre, (2) Asiatic and (3) American. After Bliokh et al. (1980)

According to Bliokh et al. (1980), it is common to distinguish two main components of the noise in the lower audio band. The first component is the continuous background level due to the global sum of all (incoherent) sources. The spectral variance of such noise is remarkably stable and remains almost constant over time intervals of the order of 1–2 h; it gives rise to the diurnal pattern noted above. The second main component is an ELF transient event which is the response of the cavity to a single, very powerful lightning discharge. The amplitude of such events can exceed the background level by a substantial factor (e.g. $>10$) and their duration is typically a few cycles. Such events may be coherent over most, if not all, of the Earth. It is these two main components that we will consider in the present study.

The structure of the ELF spectrum (i.e. the relative amplitude and the position of spectral peaks) is strongly dependent on the range from source to receiver. With simplifying assumptions concerning the source spectrum, the range of a lightning discharge is determined by comparing the recorded spectrum with spectra calculated for different ranges (Jones and Kemp, 1970). To locate a lightning discharge it is then sufficient to obtain the angle of arrival (or bearing) of the wave from the two horizontal magnetic components (Kemp, 1971). If the source spectrum is not simple (i.e. it may comprise multiple return discharges), the received spectrum will be highly structured and the above procedure is difficult to apply. This particular problem can be overcome by using the spectrum of the wave impedance ($E_r/H_\theta$), if all three electromagnetic components are measured (Kemp and Jones, 1971; Ingmann et al., 1985). We note that if measurements of the radial electric field ($E_r$) were routinely included in the AMT instrumentation, the exclusion of local or regional sources would, in theory at least, be possible. If $E_r$ is not observed, the simplest source characteristic to investigate is the bearing of the wave by a

polarization analysis of the two horizontal magnetic components.

### Polarization analysis of Schumann waveforms

Some of the data used in the present analysis were used in the spectral study of Beamish and Tzanis (1986). The instrumental conditioning and collection scheme provides four decades of data from 100 to 0.01 Hz. Decade 1 is sampled at 400 Hz and resampled at 200 Hz, providing a data bandwidth from 100 to 10 Hz. This decade attenuates the fundamental (7.5 Hz) Schumann resonance mode but provides data for studies of the higher-order modes. It is data from this decade that are used in the present study. The data were collected in western Anatolia (Turkey), geographic coordinates 40.5° N, 30° E. The spectral content of typical decade-1 data has been described by Beamish and Tzanis (1986).

A large number of individual data windows were collected at a number of sites. We present detailed examples of waveform characteristics on two separate days, at two separate locations. The three examples from the first day (8 June 1984, between 10:40 and 11:00 L.T.) have relatively uniform variance and can be considered representative of the ELF background field. They are referred to as events B1, B2 and B3. The three examples from the second day (27 July 1984, between 10:37 and 10:50 L.T.) are impulsive waveforms having peak-to-peak amplitudes of between $\times 5$ and $\times 15$ that of the background level and are considered representative of typical ELF events. They are referred to as events I1, I2 and I3. The waveforms recorded can display a high degree of amplitude/frequency variance as typified in the four equivalent sonograms of Fig. 2. This figure shows the spectral content of successive data windows in the N–S horizontal magnetic field of decade-1 data. In general, the Schumann resonance waveforms comprise "events" superimposed on a background. In order to extract realistic polarization parameters for the waveforms considered, it has been necessary to investigate time-local polarization analysis techniques.

In the present study we adopt a technique, proposed by Kodera et al. (1977) and first described by Gabor (1946), which permits the derivation of the polarization parameters in the time domain in the form of instantaneous values. This procedure has the advantage of tracing any variation in the state of polarization of *individual* waveforms encountered within a particular data window. The technique extends the formalism obeyed by a complex signal $c = x + iy$, associated with any two orthogonal components $x$ and $y$, to a two-component representation. Kodera et al. (1977)

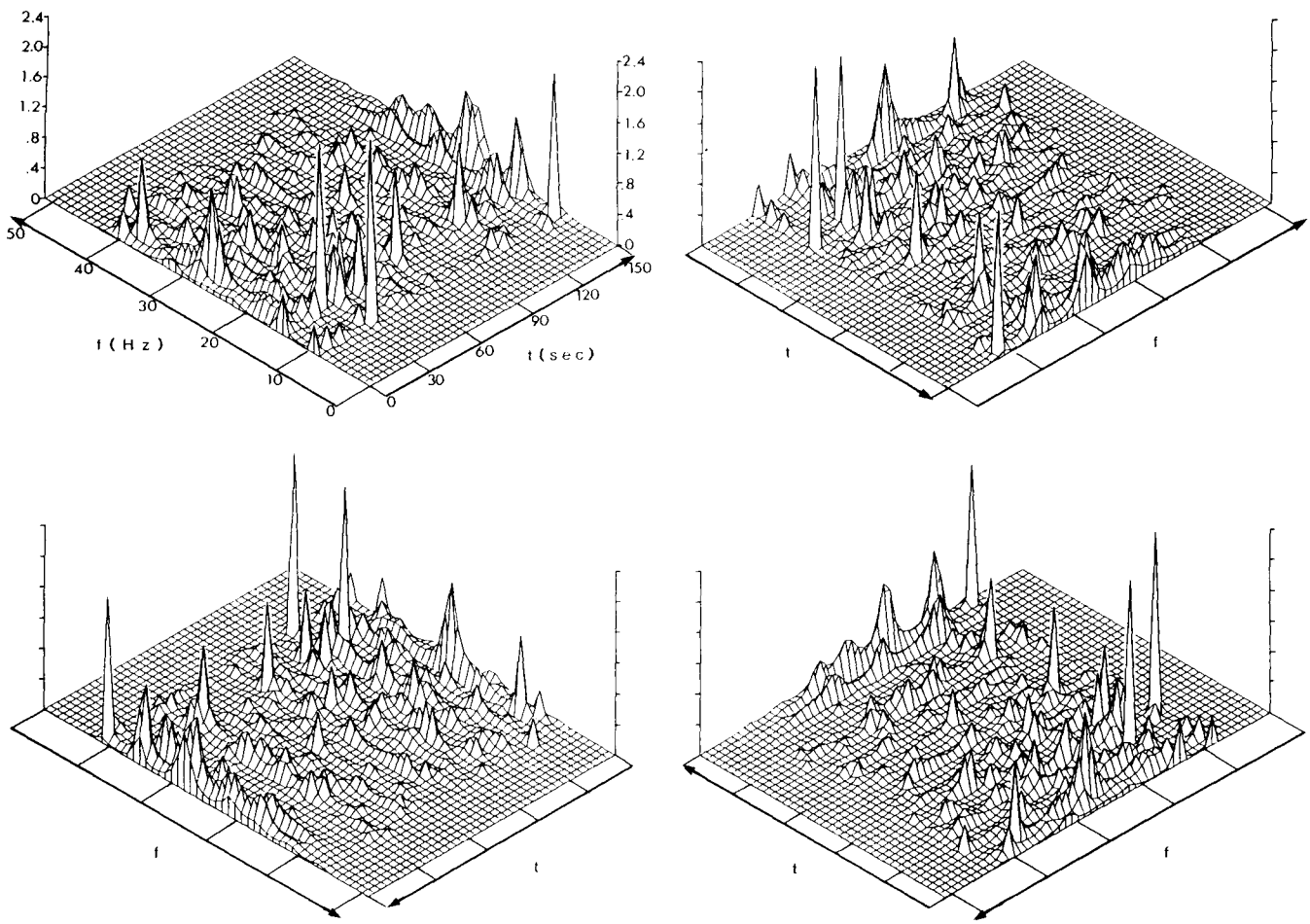


**Fig. 2.** High-resolution sonogram of the N–S ($H_x$) magnetic component. Four perspective view of the *same* sonogram. Data collected on 8 June 1984. Power density values in $(\text{nT})^2\,\text{Hz}^{-1} \times 10^{-6}$. Decade-1 data, 10–100 Hz. Maximum entropy power spectra. Filter length $M = 35$

demonstrate that it is possible to decompose the complex signal in terms of circular components rotating in opposite directions. At any given frequency $f_0$, we may write:

$$c(t, f_0) = C(w_0) \exp(i w_0 t),$$

which represents a circular harmonic in the complex plane, rotating in a sense which depends on the sign of $w_0$. Positive (+) frequencies correspond to circular components rotating in the counterclockwise direction and negative (−) frequencies to components rotating in the clockwise sense. The power spectrum of the complex signal is related to the intensity of the circular components and the spectral asymmetry to the polarization of the real signals. The authors detail how the two complex circular decomposites of the complex signal can be written in terms of the equivalent real decomposites of the two orthogonal components, in the form:

$$c^+(t) = x^+(t) + iy^+(t),$$
$$c^-(t) = x^-(t) + iy^-(t).$$

By introducing the concept of the complex *analytic* signal associated with any real signal (e.g. Ville, 1946), one can easily show that:

$$x^+(t) = x_a(t)/2 \qquad x^-(t) = x_a^*(t)/2$$

and similarly for the $y$ component. The subscript $a$ denotes the analytic signal; the asterisk, complex conjugation. Consequently, one can deduce that:

$$c^+(t) = [x_a(t) + iy_a(t)]/2,$$
$$c^-(t) = [x_a^*(t) + iy_a^*(t)]/2.$$

For monochromatic or quasi-monochromatic signals, the standard polarization parameters are easily obtained as:

half major axis: $a = |c^+| + |c^-|$

half minor axis: $b = |c^+| - |c^-|$

ellipticity: $\varepsilon = b/a$

azimuthal angle: $\theta = [\arg(c^+) + \arg(c^-)]/2.$

In the above expressions, $b$ and $\varepsilon$ are positive for counterclockwise rotation and negative for clockwise rotation. We use a different numerical implementation to that suggested by Kodera et al. (1977), which appears to be more suitable for data displaying large waveform variability. This has been described in Tzanis and Beamish (1986b).

The same method of presentation is repeated for all six examples. Events B1, B2 and B3 (background field) consist of 150 data points in ($H_x$, $H_y$). The time interval considered is 0.75 s. Events I1, I2 and I3 consist of 50 data points (0.25 s) in ($H_x$, $H_y$). For each example, the two-component data are displayed first. The polarization parameters ellipticity ($\varepsilon$) and azimuth ($\theta$) are then displayed in the time domain, below the corresponding data. The instantaneous values of $\varepsilon$ and $\theta$ consist of a series of discrete symbols that correspond to the extrema in ($H_x$, $H_y$), i.e. the signal inflexion points, evaluated using the modulus. If the amplitude of the modulus falls below a pre-set threshold (usually taken as a percentage amplitude of the maximum excursion encountered), the result is omitted. This is a simple and effective method of rejecting noise. The thresholds used here are of the order of 25% for the background field and 10% for the ELF transient events. In keeping with the previous definitions, a value of $\varepsilon = 1$ corresponds to a circular wave rotating in a counterclockwise (+) sense, a value of $\varepsilon = 0$ corresponds to a linearly polarized wave and a value of $\varepsilon = 1$ to a circular wave rotating in a clockwise (−) sense. Azimuths are defined as magnetic west (180°), magnetic north (90°) and magnetic east (0°).

Figure 3a shows the results from the analysis of event B1. There are no strongly dominant waveforms and the peak-to-peak amplitudes are less than 0.01 nT. A high degree of variability in polarization characteristics is apparent. Figure 3b shows the results obtained from event B2. Peak-to-peak amplitudes are all less than 0.02 nT. The large $H_y$-component waveform is clearly linearly polarized, while the other waveforms display a variety of polarization characteristics. Example B3 (Fig. 3c) is not totally representative of the background field due to the presence of a large-amplitude waveform (just after 0.50 s), possessing a larger variance level and more stable polarization characteristics as a function of time. This example can be directly compared with the impusive waveforms shown in Fig. 4. It is easily recognized that the three main impulsive waveforms shown in Fig. 4 all posses a near-zero initial ellipticity but distinctly different azimuths. The azimuths of examples I1 and I2 differ by 66°; the azimuths of I2 and I3 by 60°. All waveforms possess similar amplitudes. The real time interval between I1 and I3 is approximately 8 min.

Our purpose in presenting the above results has been to provide typical examples of the polarization characteristics of ELF waveforms. The spectral content of these data indicate that the waveforms are due to the Schumann resonances, originating in the Earth-ionosphere cavity (Beamish and Tzanis, 1986). The most straightforward use of the polarization characteristics presented is the identification of the bearing of the source. The horizontal bearing of the source is perpendicular to the polarization azimuth of the horizontal magnetic field. The bearings of the background waveforms display the prescribed level of variability for incoherent sources with two exceptions. The two larger-amplitude waveforms in Fig. 3b and c are both characterised as short-duration, quasi-linear waveforms. Their amplitude excursion exceeds the background by a factor of less than 5 and the bearings of the two sources appear in opposite quadrants. Their polarization characteristics appear to be a more stable function of time. The three main impulsive events considered in Fig. 4 appear a simple, damped quasi-sinusoidal oscillations. These waveforms posses the characteristic commencement of typical transient events, interpreted by Jones and Kemp (1970) as the response of the cavity to single, powerful and relatively short-duration lightning discharges. The initial portion of any ELF disturbance is due to the direct reception of radiation from the discharge. Subsequent fluctuations are due the circulation of energy around the globe. For genuinely impulsive waveforms, the onset should be characterised by an ellipticity of zero. This feature is common to the three transient events analysed. The two "main" waveforms encountered in Fig. 4b are a good example of source "repetition" on a time scale of 0.25 s. The same effect is also evident in Fig. 4a. Another interesting feature in this figure is the existence of a small-amplitude waveform just prior to the onset of the main impulsive event, with distinctly different polarization characteristics ($\theta = 87°$, $\varepsilon = 0.25$). The results demonstrate the extremely time-local behaviour of the ELF sferic waveforms. When the bearings of the three impulsive forms of Fig. 4 are compared, it is apparent that the sources have different azimuthal locations. The study by Tzanis

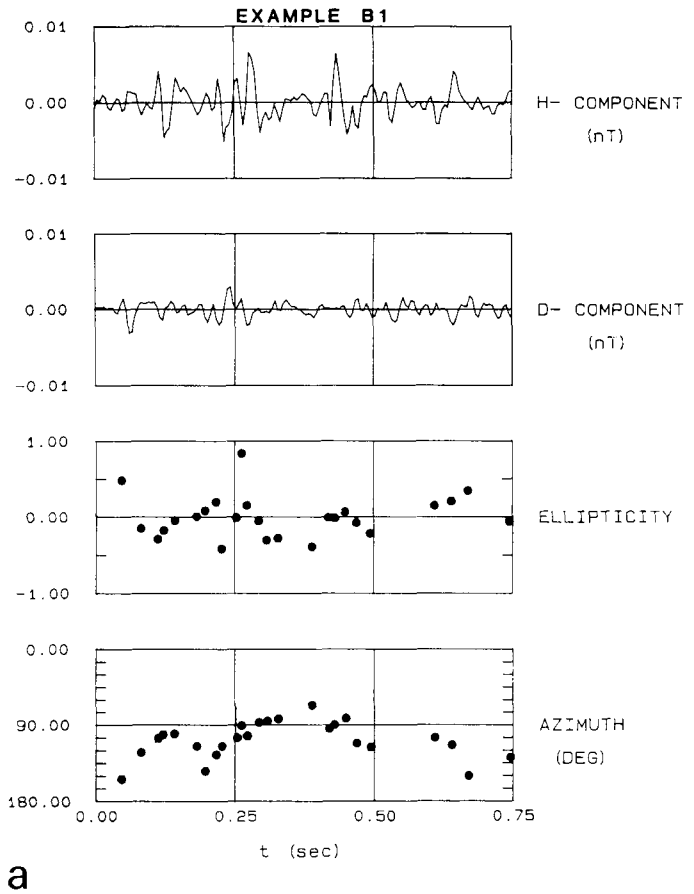


a

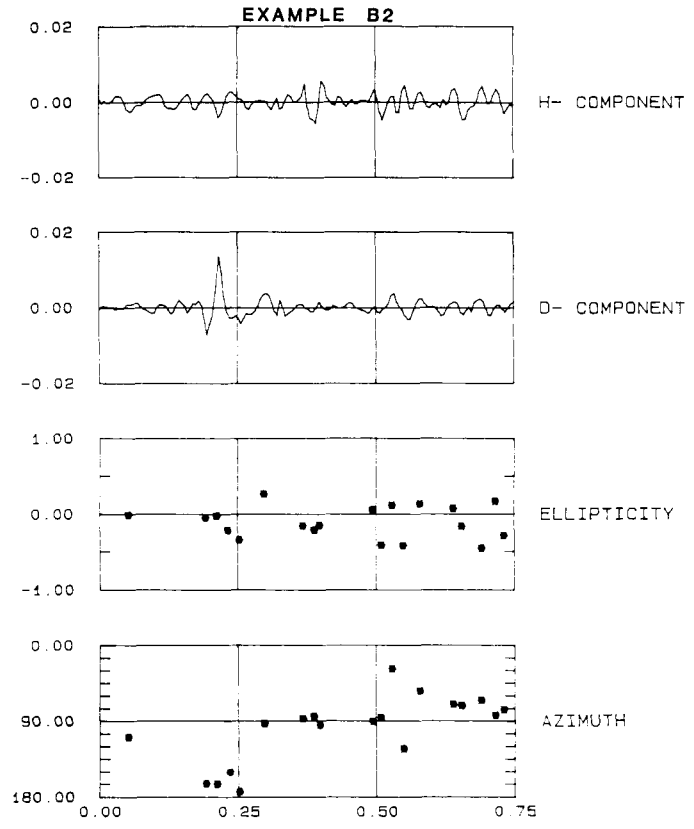


b

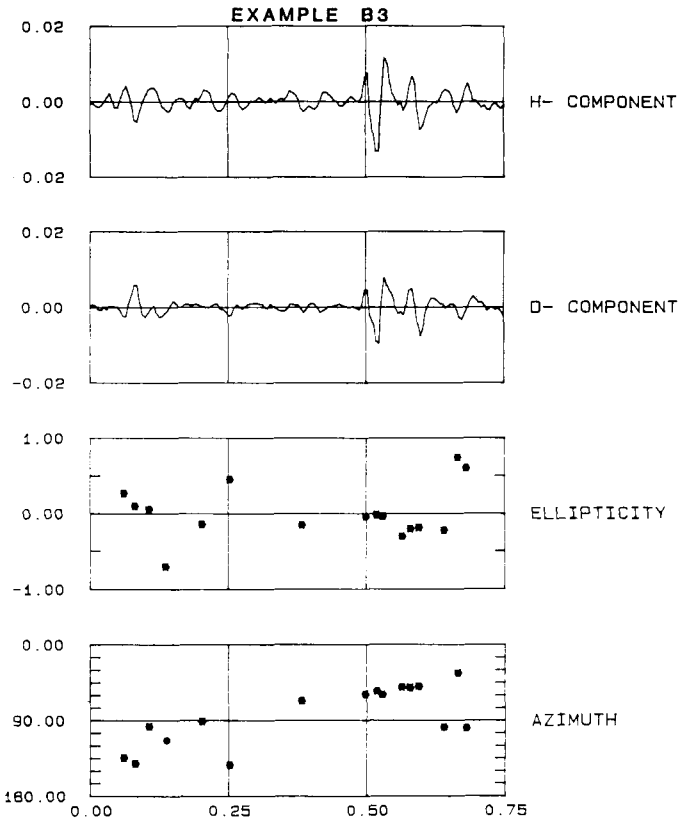


c

**Fig. 3a–c.** Three examples of the time-domain polarization analysis of background sferics. *H* and *D* correspond to the N–S and E–W magnetic components. **a** example B1; **b** example B2; **c** example B3

and Beamish (1986a) indicates that the source locations of such waveforms possess ranges (*D*) of the order of several thousand kilometres and are widely distributed across the globe. The same is evident from the data presented in this analysis; individual sources are detectable even at the background level (e.g. examples B1 and B2). The low *Q* factors (less than 8) calculated from the power spectra of the ELF sferics also indicate that energy has propagated over large distances in the Earth-ionosphere cavity. They reflect the effect of the low transmission coefficient of the cavity resonator (Bliokh et al. 1980) and can be used as a diagnostic aid in verifying the nature of the received waveforms. In conclusion, the above observations point towards the validity of the plane-wave assumption when using 'typical' Schumann resonance waveforms.

### Geoelectric sounding curves from single events

In general terms it appears that the Schumann resonances provide two main types of source waveforms for use in geoelectric sounding. The background source fields possess uniform, but low, variance and provide a complete range of source azimuths and ellipticities on time scales equivalent to the duration of the waveforms. The large-amplitude transient events are of short duration (typically less than 0.25 s) and appear as quasi-linearly polarized waveforms at a given

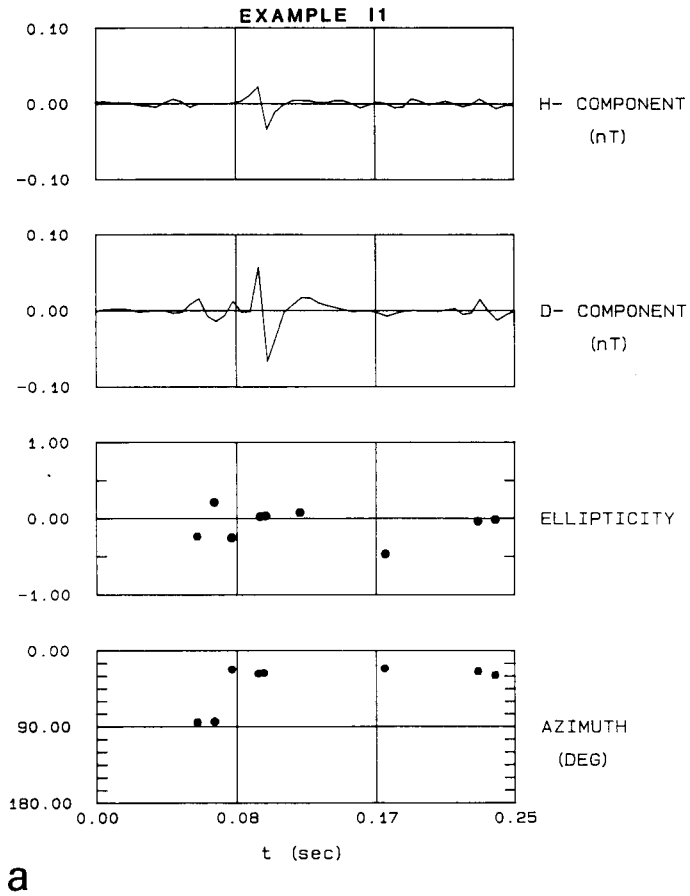


a

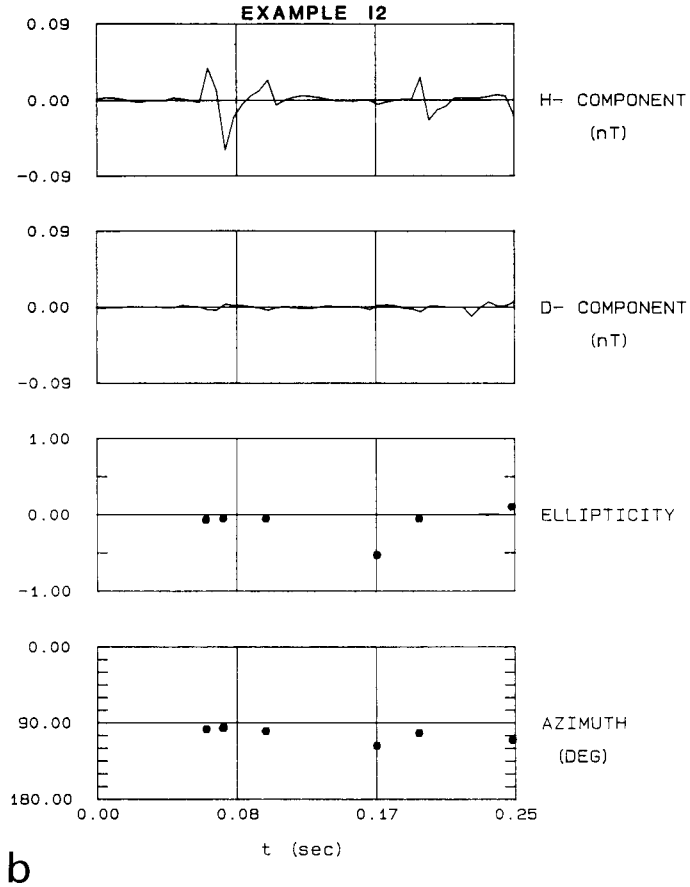


b

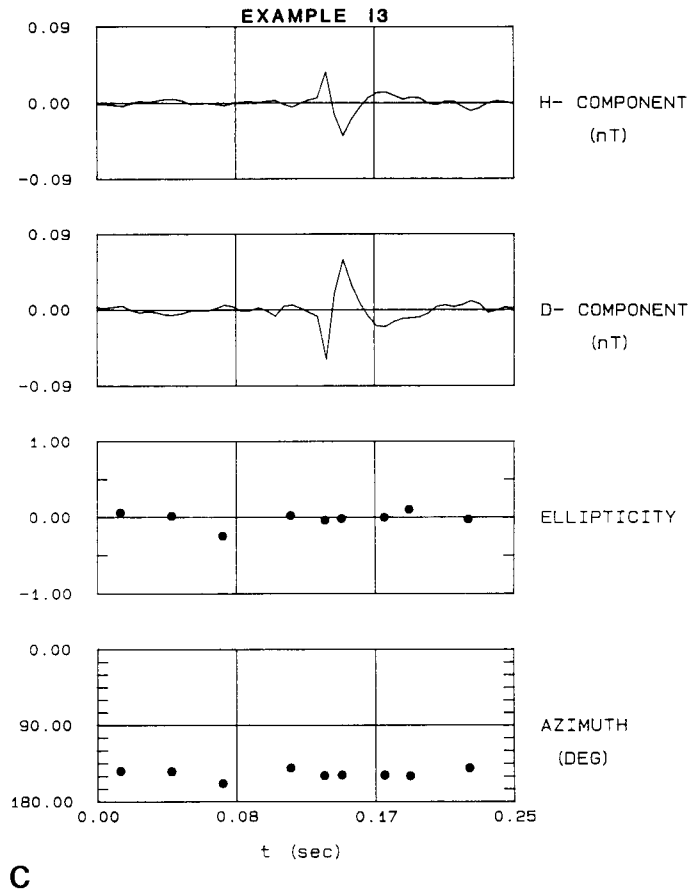


c

**Fig. 4a–c.** Three examples of the time-domain polarization analysis of ELF transient events. *H* and *D* correspond to the N–S and E–W magnetic components. **a** example I1; **b** example I2; **c** example I3

azimuth. The transient "events" available in the data provide a wide variety of such azimuths. Impulsive sources are clearly valuable for geoelectric sounding in that they possess a substantial increase in the signal-to-noise (S/N) ratio when compared with background sources. At least two source-field polarizations are required to adequately sound general 3-dimensional geoelectric structures. The use and effects of polarized source fields has been described by Hermance (1973), Lienert (1980) and Pedersen and Svennekjaer (1984). From the preceding discussion it is evident that the Schumann resonance waveform characteristics are associated with distinct azimuthal locations and propagation paths. We now proceed to investigate the extent to which such waveforms can provide repeatable geoelectric sounding curves, i.e. whether the waveform type and its particular polarization characteristics can possibly influence the determination of the Earth response. We are *not* concerned here with noise effects; thus, we deliberately choose examples with small noise content. A high (frequency-time) resolution technique is applied to sferic waveforms. This enables the response due to *individual* waveforms, directly related to a given discharge source and propagation path, to be determined.

### Data analysis and spectral estimation procedures

The data analysis follows the conventional procedures described by Vozoff (1972). The electric and magnetic field

components are related, in the frequency domain, by the two equations:

$$E_x(w) = Z_{xx}(w)\, H_x(w) + Z_{xy}(w)\, H_y(w), \quad (1)$$

$$E_y(w) = Z_{yx}(w)\, H_x(w) + Z_{yy}(w)\, H_y(w) \quad (2)$$

or, in matrix form, as $E = Z \cdot H$, where $E = [E_x\ E_y]^T$, $H = [H_x\ H_y]^T$ and $Z$ is termed the impedance tensor. The two pairs of impedance elements are usually estimated by least-squares solutions which minimize noise on a particular data channel (Sims et al., 1971). The quality of the least-squares solutions for each of the the two pairs of impedance elements is then obtained from the multiple (predicted) coherence function between a measured electric field component and that predicted by the least-squares solution.

The auto- and cross-spectral estimates between the field components are conventionally computed using the Fast Fourier Transformation (FFT) technique. Given the inherent variance of the resulting raw spectral density function, smoothing over a frequency interval (often arbitrarily chosen) is usually prescribed in order to stabilize the spectral density estimates. The frequency resolution of the resulting impedance estimates is thus drastically reduced. Additional disadvantages of the procedure are that the resulting (smoothed) spectral estimates contain the contributions of several (and often unconforming) frequency-local properties over the interval of smoothing, and that the FFT cannot handle short data lengths without loss of statistical significance in the spectral estimator. To obtain highly resolved and statistically robust impedance estimates that display properties localized in frequency, a different spectral approach can be adopted.

It appears that for the case of spectral estimation from a stationary time series, there exists a ubiquitous possibility that we can represent the time series by an autoregressive (AR) process of the form:

$$x(t) = \sum_m a(m)\, x(t-m) + e(t)$$

(Ulrych and Bishop, 1975; Jaynes, 1982), where $e(t)$ is a white-noise error series and $a(m)$ is an absolutely summable filter. Using such a model, it is possible to improve frequency resolution by determining the spectrum from the properties of the filter $a(m)$, $m = 0, .., M$ that best adapts to the given data set. The problem of spectral estimation then reduces to that of determining the optimum filter coefficient vector. Burg (1968) proposed a method for estimating the filter coefficients and hence the power spectrum of a stationary time series in the maximum entropy (ME) sense. Beamish and Tzanis (1986) demonstrated the capacity of the algorithm for the production of high-resolution spectra when applied to single-component Schumann resonance waveforms (i.e. the univariate case). In order to apply the same spectral technique to impedance estimation we require to calculate both auto- and cross-spectral estimates (i.e. the multivariate case).

Consider a vector time series of the form:

$$x(t) = [x_1(t)\, x_2(t) \ldots x_p(t)]^T, \quad t = 1, \ldots, N$$

consisting of $p$ simultaneous data channels. The equivalent linear AR system will now assume the form:

$$x(t) = \sum_m a^T(m)\, x(t-m) + e(t)$$

where $e(t)$ is a $p$ vector white-noise series and $a$ is a $p \times p$ vector absolutely summable filter. The power density spectrum will be given by the expression:

$$s(z) = \Delta t \cdot [A(z)^{-1}]^{*T} \cdot P_m \cdot [A(z)^{-1}]$$

where $P_m$ is the $p \times p$ vector residual error power and $A(z)$ is the $p \times p$ vector z-transform of the filter $a$. $\Delta t$ is the data sampling rate and the asterisk denotes complex conjugation. The least-squares minimization of $e(t)$, to provide the optimum unit prediction error filter $a$, has been considered by a number of authors (e.g. Strand, 1977; Morf et al., 1978) in a more or less direct generalization of Burg's algorithm. The simultaneous treatment of $p$ data channels provides the opportunity for a direct evaluation of both auto- and cross-spectral components using the $p \times p$ operator $a$.

For our data consider the vector time series

$$x(t) = [E_x(t)\ E_y(t)\ H_x(t)\ H_y(t)]^T, \quad t = 1, \ldots, N,$$

consisting of four data channels. The above spectral procedure is then used to form the spectral components required for the least-squares solutions. The spectral analysis algorithm implemented is a modification of the one due to Strand (1977). The estimation of the error associated with the resulting impedance tensor elements was performed according to Pedersen (1982). In the latter, the statistical significance of the principal-component spectral density estimates involved is introduced through their associated number of degrees of freedom; their distribution is assumed to be complex normal for the raw spectral density matrix and complex Wishart for its smoothed equivalent (e.g. Priestley, 1981, pp. 693–701). This is true for spectra calculated with the conventional techniques; however, the multivariate ME spectral estimator lacks an exact statistical description of its properties.

Progress can be made if we consider the statistics of the generalized linear regression system. Its spectral density matrix is shown to comprise a class of consistent, asymptotically unbiased and asymptotically complex normally distributed estimates (e.g. Brillinger, 1981, Chapter 8). It is therefore conceivable that the multivariate AR spectral estimator, being a particular case of such a system, will possess similar statistical properties, although the moments of the distribution are yet to the specified. Such an argument is based on, and enhanced by, the fact that all the entries in the data vector $x$ are assumed to be second-order stationary time series, jointly normally distributed; this somehow prescribes the result. The number of degrees of freedom associated with the principal components of the spectral density matrix are taken to be $n = N/M$, as a direct generalization of the result by Kromer (1970) concerning the statistics of the univariate AR spectral estimator. The latter was found to be unbiased, consistent and asymptotically normally distributed. The above arguments provide, at best, an approximation. However, they are based on reasonable assessments and are practical with respect to applications in EM field data analysis. A quantitative measure of the goodness of the least-squares solutions for a high-resolution (quasi-continuous) $Z$ can thus be afforded. A detailed description of the rationale and implementation of the above procedure to AMT data will be reported elsewhere.

## Results

The particular solution we use here for demonstration assumes that the noise exists only in the electric field components and is referred to as a downward-biased estimate.

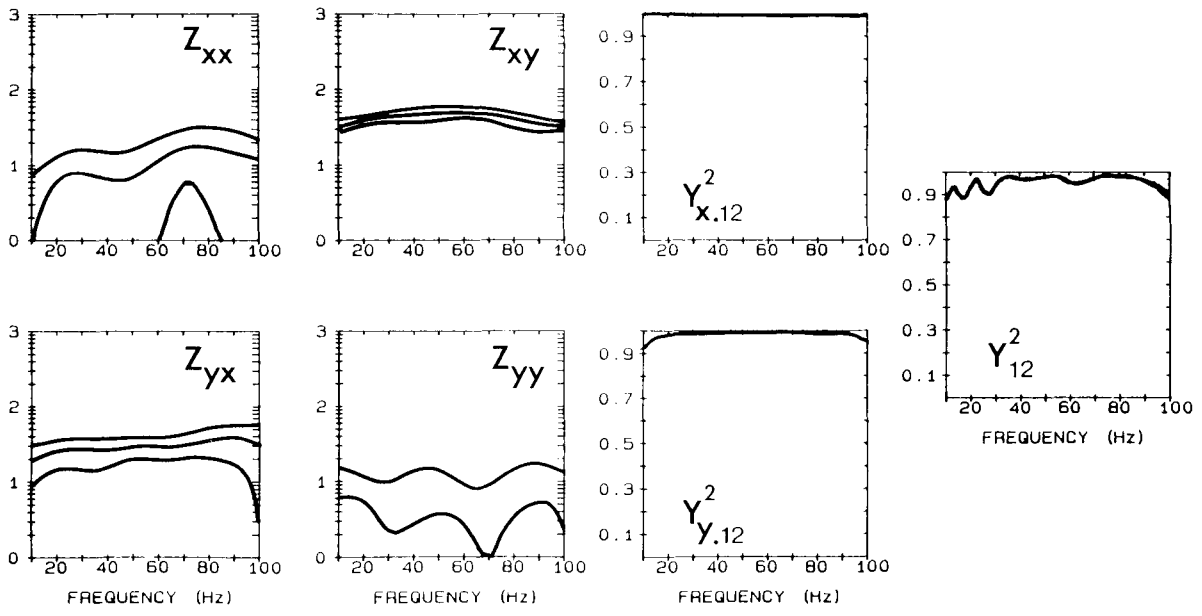


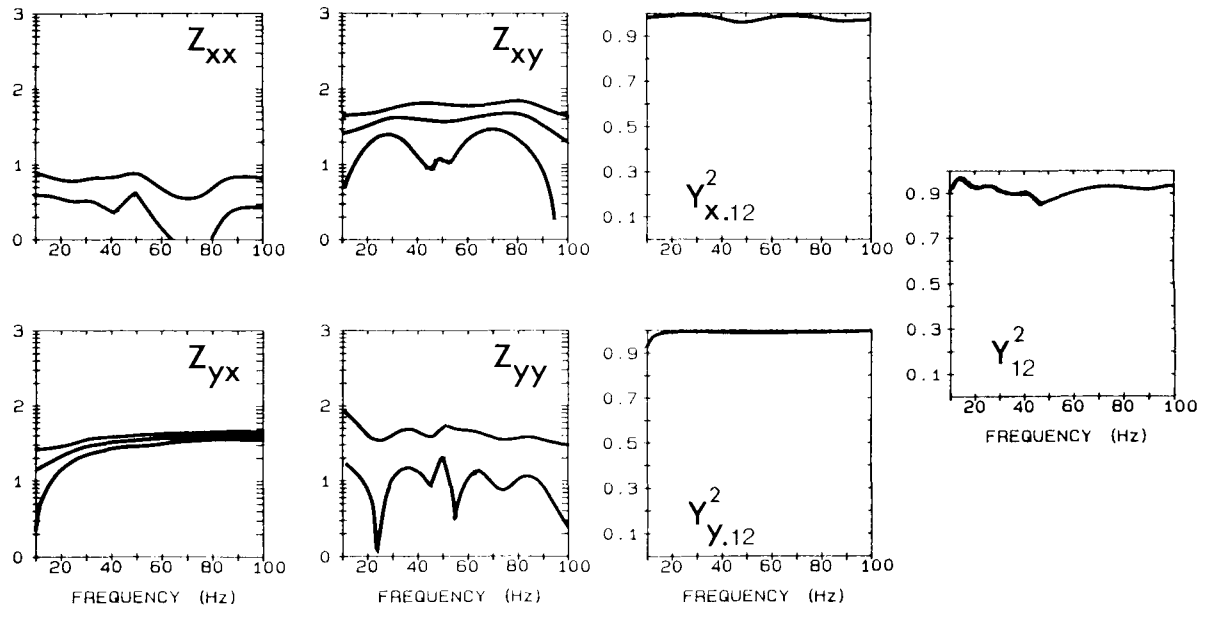


**Fig. 5a–c.** Three examples of the downward-biased impedance tensor elements, calculated from high-quality ELF *transient events* with the multivariate ME method. Analysis parameters are $N=50$ (0.25 s), $M=6$. 58 frequency estimates, 1.56 Hz apart. Results are the modulus of the impedance tensor, the predicted coherence functions $Y^2_{i.12}$ and the input field ordinary coherence $Y^2_{12}$. 1 and 2 refer to the input field components $H_x$ and $H_y$, respectively. *Upper and lower curves* represent 95% confidence limits; *middle curve* is the estimated impedance

Figure 5 displays the results from three data windows containing large-amplitude ELF transient events. Figure 6 shows the equivalent results obtained from background waveforms. We present the modulus of the impedance tensor elements (logarithmic scale) as a function of frequency (linear scale), as well as the predicted coherence function ($Y^2_{i.12}$, $i=x,y$) and the input field coherence ($Y^2_{12}$). The subscripts $x$ and $y$ will henceforth refer to the predicted coherences associated with the solutions of Eqs. (1) and (2) respectively. The error bounds displayed represent the 95% confidence limits. The larger error bounds associated with the ELF transient event impedances are explained as follows. The capability of the ME method to handle short data lengths permits the analysis of such waveforms in isolation, without interference from other sources. Typically, data windows of 0.25-s (50 data points) duration have been analysed in Fig. 5. The degrees of freedom associated with the resulting spectral components are necessarily reduced

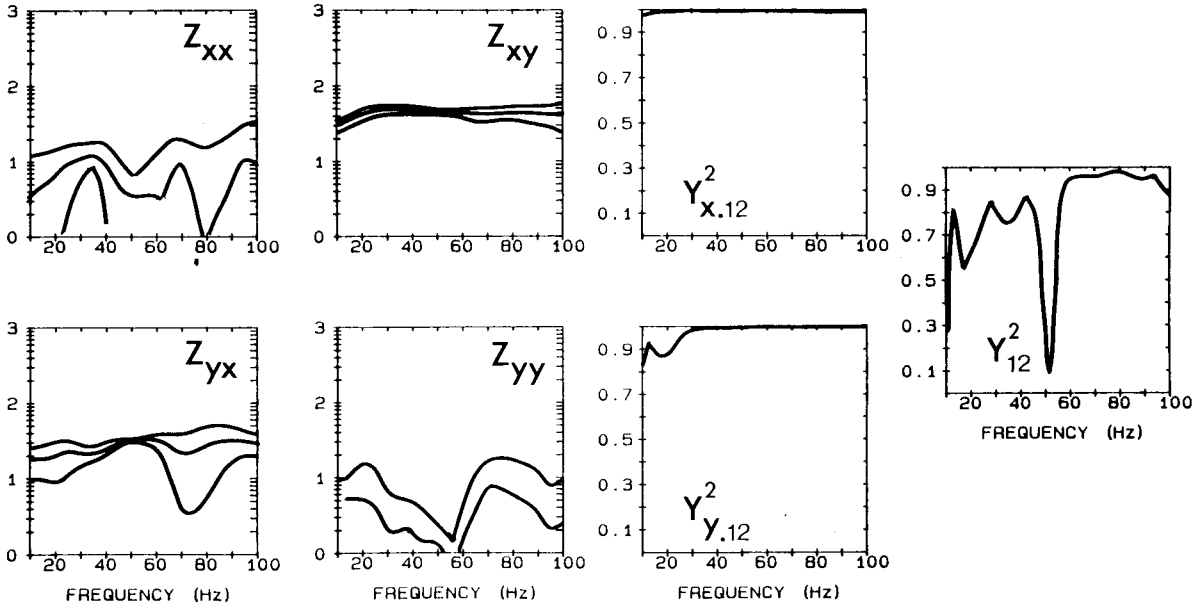


C

(e.g. $n=8$ for a filter length of $M=6$), with a corresponding widening of the confidence interval. Care should therefore be exercised when comparing the errors between the transient and the background waveform throughout this discussion; the difference may, at first glance, be misleading. In addition, the geoelectric structure of the measurement site has been identified as 2-dimensional and, by chance, the directions of the axes of measurement were almost coincident with the principal geoelectric structural directions. In such circumstances, the least-squares solutions are pathological for the diagonal elements and give rise to the instabilities observed. The data from this site permit a study of a naturally decoupled (rotated) data set. Consequently, we shall focus our attention on the off-diagonal elements.

A detailed comparison of the six results for the off-diagonal impedance pair ($Z_{xy}$, $Z_{yx}$) reveals that the estimates obtained from "single" events are consistent at the 95% confidence level. The properties which differ in the two types of waveforms analysed are the levels of predicted coherence (of both solutions) and the input field ordinary coherence. A comparison of the input field (i.e. magnetic field) ordinary coherence functions reveals that the transient events (Fig. 5) display much higher levels than do the background events of Fig. 6. The input field coherence remains large across the complete bandwidth. According to Pedersen and Svennekjaer (1984), very high $Y^2_{12}$ may be associated with high degrees of polarization of the input field; this is certainly true for the data in question. The predicted coherence functions associated with the transient events are invariably $>0.95$, so that bias in the impedance estimates is expected to be minimal. The background waveforms display a high degree of stability throughout their impedance spectra. The predicted coherence is $>0.80$ and the input field coherence $Y^2_{12}$ displays a strong frequency dependence and is generally much lower than that associated with the transient events. We interpret this as an effect of the data containing samples of several waveforms at various states of polarization, whose relative contribution produces the results shown. In summary, a comparison of the stable impedance elements from the two types of Schumann resonance activity indicates that they are consistent and that our estimation procedure is not influenced by polarization properties of the transient waveforms.

This assertion is examined in more detail by considering the results presented in Fig. 7. *Single*-frequency estimates for the four tensor impedance elements are shown. The frames indicated by "B" contain estimates from a number of background data windows, arranged as a function of a count number. The frames indicated by "I" contain estimates from ELF transient events, plotted as a function of their associated azimuthal angle. For this demonstration, azimuths are defined as 90° (magnetic east), 0° (magnetic north) and −90° (magnetic west). All the data windows that provided the results for Fig. 7 have been selected on the basis of high S/N ratio ($Y^2_{i.12}>0.85$, $i=x, y$). An additional requirement for the selection of the ELF transients analysed was waveform purity, i.e. absence of any other interfering sources. This has been achieved by analysing short data lengths. The real time interval within which these waveforms were collected is approximately 8 min. The estimates shown *between* the frames are averaged impedances. Averaging was performed by using the associated 95% confidence limits as weights. The first estimate from the left (marked with "B") is the average of the impedance elements in frame "B"; the third (marked with "I") is the equivalent for the impedances in frame "I". The second (unmarked) estimate is the combined result of a data set of 165 data windows with duration lengths of 0.75 s (150 data points), containing the whole range of possible Schumann resonance waveforms at various noise levels. Three example at frequencies 17 Hz, 25 Hz and 64 Hz are presented for demonstration. No systematic variation with azimuth, of the impedances derived from the linearly polarized waveforms, is evident. All estimates appear to be within the 95% limits of their population average.

In summary, it appears that the Schumann resonances can provide consistent and repeatable geoelectric sounding curves that are independent of the state of polarization of

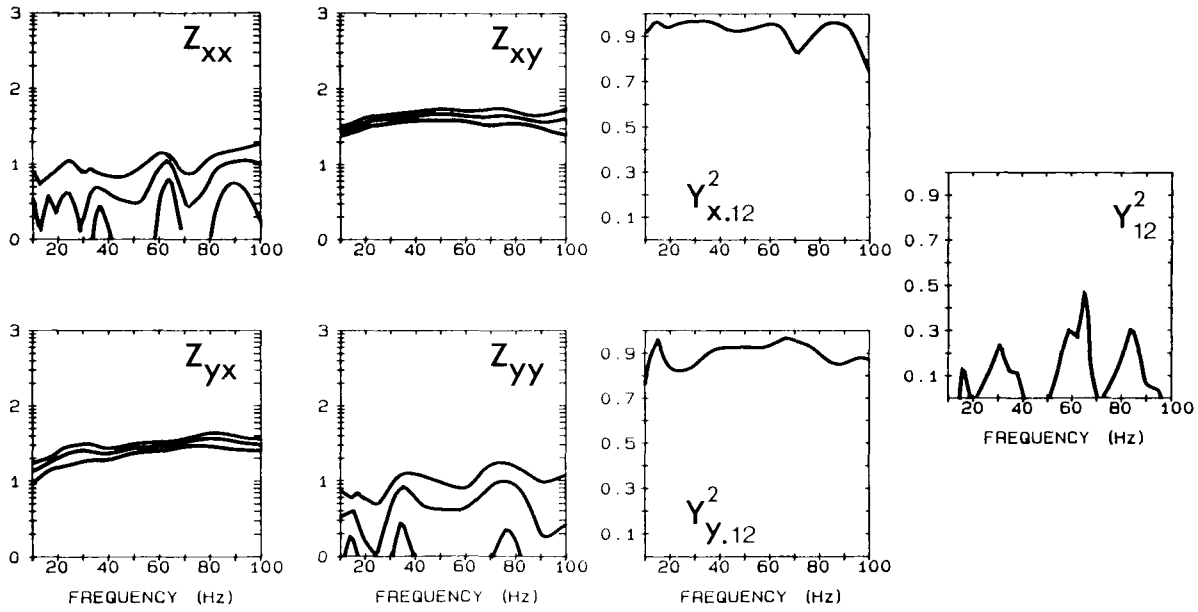


**Fig. 6a–c.** As for Fig. 5, but for high-quality ELF *background*. Analysis parameters are $N = 150$ (0.75 s), $M = 10$

the waveforms. Our results indicate that, ideally, geoelectric sounding can be performed with one or two high-quality data windows (e.g. the impulsive events of Fig. 4). The same conclusions can be drawn by considering the impedance phase results which have been omitted for the sake of brevity.

## Summary

This study has considered Schumann resonance waveforms and their applied use for sounding crustal geoelectric structure. It has been noted that such waveforms provide the main energy component as we employ higher-frequency fields and encounter the transition from a spectrum derived from geomagnetic disturbances to a spectrum ultimately dominated by ELF sferics.

The spectral characteristics noted from previous work and the waveform polarizations investigated in this study appear consistent with theoretical models of thunderstorm energy release and propagation in the Earth-ionosphere cavity. We have examined the two main components of the energy spectrum: namely, the background field and the larger-amplitude transient waveforms. By making use of the horizontal polarization properties of the waveforms it

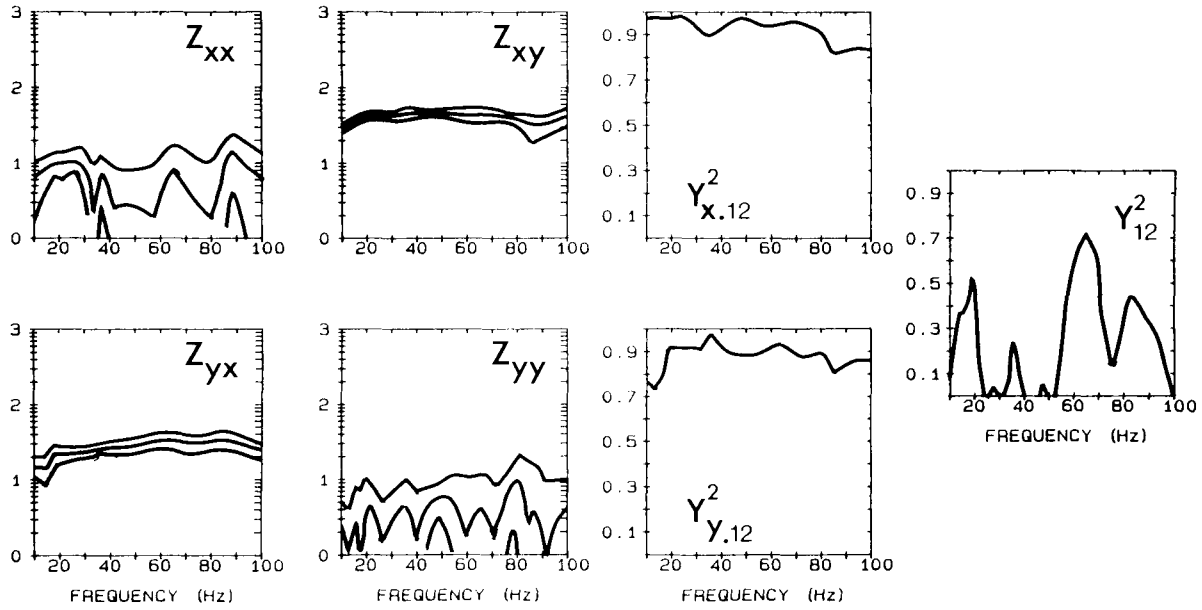


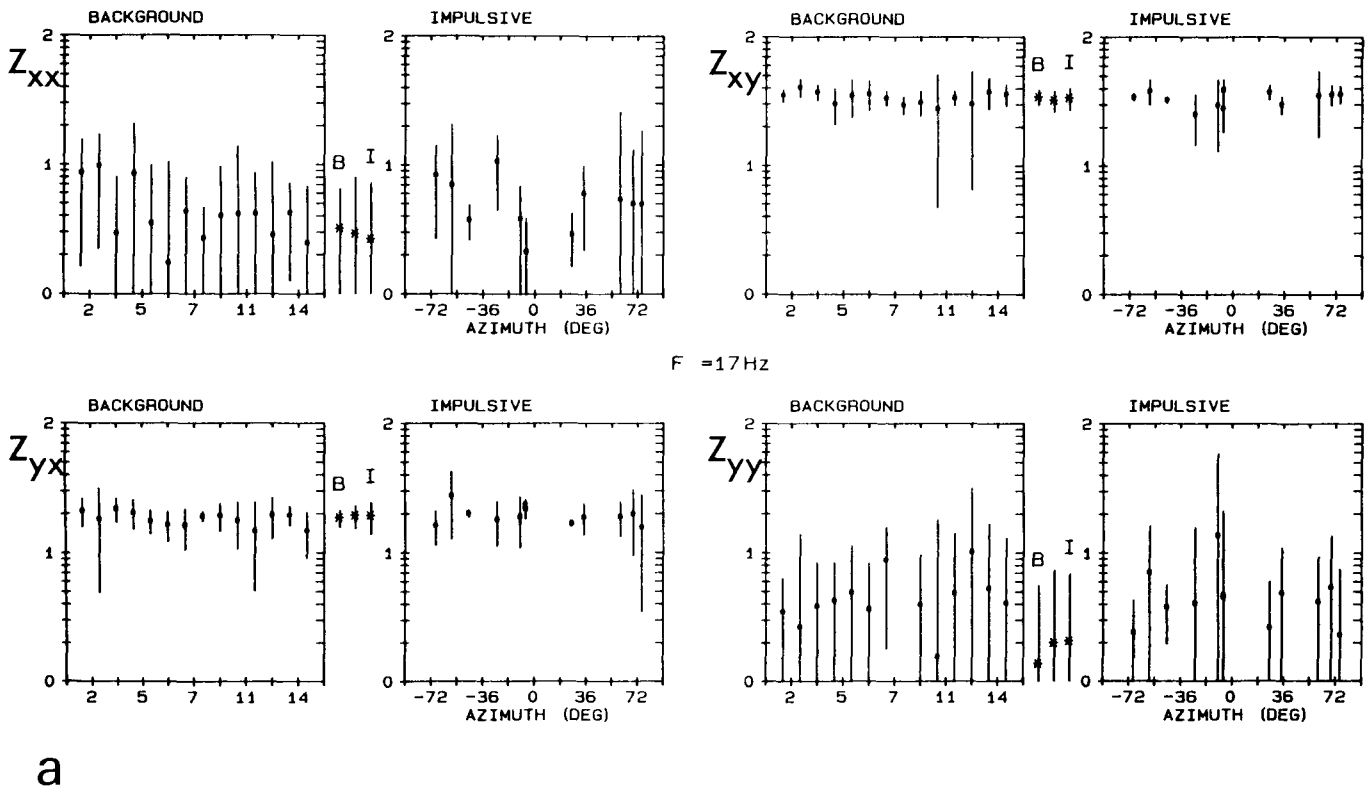


**Fig. 7a–c.** Comparison of impedance results from ELF background (*frame B*) and transient events (*frame I*). Three examples of *single-frequency* tensor estimates, calculated as for Fig. 6 and 5, respectively. Error bars are 95% confidence limits. **a** 17 Hz; **b** 25 Hz; **c** 64 Hz

has been possible to demonstrate the 'incoherent' nature of the background field and the arrival of larger energy components from individual thunderstorm centres distributed across the globe. By making joint use of the spectral and polarization properties of the waveforms it has been possible to obtain estimates of the range of source locations. Our data indicate that the larger energy components have propagated over large distances in the Earth-ionosphere cavity. The results, for both energy components, point toward the validity of the 'plane-wave' assumption.

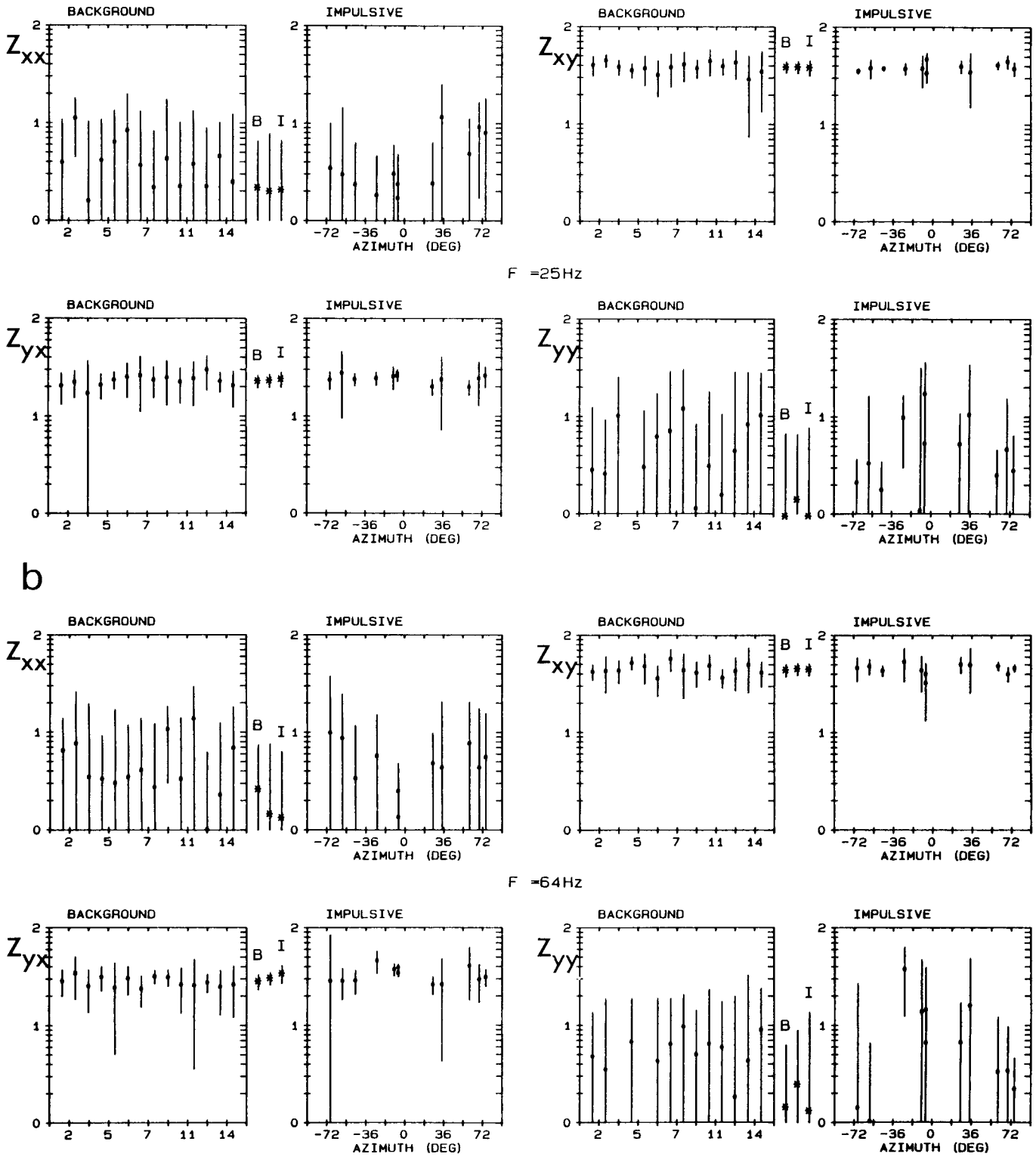


Fig. 7b, c

Our study has also considered the extent to which the Schumann resonance waveforms and their properties influence geoelectric sounding curves. In order to isolate the effects of short-duration waveforms we have found it useful to employ a maximum entropy spectral analysis scheme. Such a scheme is particularly appropriate for the transient events because it enables the geoelectric response of *individual* waveforms, directly related to a given discharge and propagation path, to be determined. Our data suggest that the two main Schumann energy components provide two

types of behaviour in the coherence functions typically determined by least-squares solutions. The background waveforms, which necessarily have the lowest S/N levels, consistently provide the lowest values in both the predicted coherence and input field ordinary coherence. When the transient events are analysed on an individual basis they are found to provide very high values in both of these coherence functions.

We have examined the behaviour of the impedance functions obtained using both types of waveform. For the background waveforms, 14 repeat determinations are shown. For the transient events 11 determinations, with the events classified according to their polarization angle, have been provided. The comparison is made for three selected frequencies. The 'individual' estimates obtained for the two types of waveform are consistent at the 95% confidence level and no systematic variation with polarization angle is evident. Using equivalent degrees of freedom, the transient events generally provide a more accurate result.

Each set of 'individual' waveform data were also combined to form 'average' results for both waveform types. The results obtained were then compared with the 'composite' results using a much larger data set comprising all waveform types. The 'individual', 'average' and 'composite' results are all entirely consistent. Our results indicate that an adequate AMT sounding for the Schumann bandwidth can be achieved using only a small number of high-quality data windows provided by the impulsive events.

*Acknowledgements.* The data collection was supported by the Natural Environment Research Council, the Overseas Development Administration and Kandilli Observatory, Bogazici University. This paper is published with the permission of the Director, British Geological Survey (NERC).

## References

Abbas, M.: Hydromagnetic wave propagation and excitation of Schumann resonances. Planet. Space Sci. **16**, 831–844, 1968

Beamish, D., Tzanis, A.: High resolution spectral characteristics of the Earth-ionosphere cavity resonances. J. Atmos. Terr. Phys. **48**, 187–203, 1986

Bliokh, H., Nikolaenko, A.P., Filippov, Yu.F.: Schumann resonances in the Earth-ionosphere cavity (Llanwyn-Jones, D., ed.). IEE Electromagnetic Wave Series 9, P. Peregrinus Ltd. 1980

Brillinger, D.R.: Time series. Data analysis and theory. Holden-Day 1981

Burg, J.P.: A new analysis technique for time series data. Paper presented at the NATO Advanced Study Institute on Signal Processing with Emphasis on Underwater Acoustics, Enschede, The Netherlands, August 1968

Gabor, D.: Theory of communication, J. Inst. Elec. Eng. **93**, 429–457, 1946

Hermance, J.F.: Processing of magnetotelluric data, Phys. Earth Planet. Inter. **7**, 349–364, 1973

Hoover, D.B., Long, C.L., Senterfit, R.M.: Some results from audiomagnetotelluric investigations in geothermal areas. Geophysics **43**, 1501–1514, 1978

Ingmann, P., Schaefer, J., Volland, H., Schmolder, M., Manes, A.: Remote sensing of thunderstorm activity by means of VLF sferics, PAGEOPH **123**, 155–170, 1985

Jaynes, E.T.: On the rationale of maximum entropy methods. Proc. IEEE. **70**, 939, 1982

Jones, D.L., Kemp, D.T.: Experimental and theoretical observations of transient excitation of Schumann resonances. J. Atmos. Terr. Phys. **32**, 1095–1108, 1970

Keller, G.V.: Natural-field and controlled-source methods in electromagnetic exploration. Geoexploration **9**, 99–147, 1971

Keller, G.V., Frischknecht, F.C.: Electrical methods in geophysical prospecting. Pergamon Press 1966

Kemp, D.T.: The global location of large lightning discharges from single station observations of ELF disturbances in the Earth-ionosphere cavity. J. Atmos. Terr. Phys. **33**, 919–928, 1971

Kemp, D.T., Jones, D.L.: A new technique for the analysis of transient ELF electromagnetic disturbances within the Earth-ionosphere cavity. J. Atmos. Terr. Phys. **33**, 567–572, 1971

Kodera, K., Gendrin, R., De Villedary, C.: Complex representation of a polarized signal and its applications to the analysis of ULF waves. J. Geophys. Res. **82**, 1245–1255, 1977

Kromer, R.: Asymptotic properties of the autoregressive spectral estimator. Ph.D. thesis, Dept. of Statistics, Stanford Univ., Stanford, California, 1970

Labson, V.F., Becker, A., Morrison, H.F., Conti, U.: Geophysical exploration with audiofrequency natural magnetic fields. Geophysics **50**, 656–664, 1985

Lienert, B.R.: The effect of source field polarization on estimates of the magnetotelluric impedance tensor. Geophysics **45**, 1803–1812, 1980

Madden, T., Thomson, W.: Low-frequency electromagnetic oscillations of the Earth-ionosphere cavity. Rev. Geophys. **3**, 211–254, 1965

Morf, M., Vieira, A., Lee, D.T.L., Kailath, T.: Recursive multichannel maximum entropy spectral estimation. IEEE Trans. on Geoscience Electronics **GE-16**, 85–94, 1978

Pedersen, L.B.: The magnetotelluric impedance tensor – its random and bias errors. Geophys. Prospect. **30**, 188–210, 1982

Pedersen, L.B., Svennekjaer, M.: Extremal bias coupling in magnetotellurics. Geophysics **49**, 1968–1978, 1984

Priestley, M.B.: Spectral analysis and time series – Volume 2: multivariate series, prediction and control. Academic Press 1981

Russell, C.T., Holzer, R.E., Smith, E.J.: OGO 3 observation of ELF noise in magnetosphere, II. The nature of equatorial noise. J. Geophys. Res **75**, 755, 1970

Sims, W.S., Bostick Jr, F.X., Smith, H.W.: The estimation of magnetotelluric impedance tensor elements from measured data. Geophysics **36**, 938–942, 1971

Slankis, J.A., Telford, W.M., Becker, A.: 8-Hz telluric and magnetotelluric prospecting. Geophysics **37**, 862–878, 1972

Strand, O.N.: Multichannel complex maximum entropy (autoregressive) spectral analysis, IEEE Trans. on Autom. Control **AC-22**, 634–640, 1977

Strangway, D.W., Swift Jr, C.M., Holmer, R.C.: An application of audio frequency magnetotellurics (AMT) to mineral exploration. Geophysics **38**, 1159–1175, 1973

Telford, W.M.: Characteristics of audio and sub-audio telluric signals. Geophys. Prospect. **25**, 321–333, 1977

Tzanis, A., Beamish, D.: Time domain polarization analysis of Schumann resonance waveforms. J. Atmos. Terr. Phys. 1986a (in press)

Tzanis, A., Beamish, D.: Observations of the polarization properties of sferic waveforms. GRG Internal Report 86/13, British Geological Survey, 1986b

Ulrych, T.J., Bishop, T.N.: Maximum entropy spectral analysis and autoregressive decomposition. Rev. Geophys. Space Phys. **13**, 183–200, 1975

Uman, M.A.: Lightning, McGraw-Hill 1969

Ville, J.: Theorie et applications de la notion de signal analytique. Cables Transm. **1**, 61–74, 1946

Vozoff, K.: The magnetotelluric method in the exploration of sedimentary basins. Geophysics **37**, 98–114, 1972

Watt, A.D.: VLF radio engineering. Pergamon Press 1967

Received November 11, 1986; revised version February 5, 1987
Accepted February 13, 1987